The Cryosphere, 6, 1163–1174, 2012
www.the-cryosphere.net/6/1163/2012/
doi:10.5194/tc-6-1163-2012

The Cryosphere

P-wave velocity changes in freezing hard low-porosity rocks: a laboratory-based time-average model

D. Draebing and M. Krautblatter

Department of Geography, Bonn, Germany

Correspondence to: D. Draebing (daniel.draebing@giub.uni-bonn.de)

Received: 26 January 2012 – Published in The Cryosphere Discuss.: 21 February 2012
Revised: 6 September 2012 – Accepted: 16 September 2012 – Published: 22 October 2012

Abstract. P-wave refraction seismics is a key method in permafrost research but its applicability to low-porosity rocks, which constitute alpine rock walls, has been denied in prior studies. These studies explain p-wave velocity changes in freezing rocks exclusively due to changing velocities of pore infill, i.e. water, air and ice. In existing models, no significant velocity increase is expected for low-porosity bedrock. We postulate, that mixing laws apply for high-porosity rocks, but freezing in confined space in low-porosity bedrock also alters physical rock matrix properties. In the laboratory, we measured p-wave velocities of 22 decimetre-large low-porosity (< 10 %) metamorphic, magmatic and sedimentary rock samples from permafrost sites with a natural texture (> 100 micro-fissures) from 25 °C to −15 °C in 0.3 °C increments close to the freezing point. When freezing, p-wave velocity increases by 11–166 % perpendicular to cleavage/bedding and equivalent to a matrix velocity increase from 11–200 % coincident to an anisotropy decrease in most samples. The expansion of rigid bedrock upon freezing is restricted and ice pressure will increase matrix velocity and decrease anisotropy while changing velocities of the pore infill are insignificant. Here, we present a modified Timur's two-phase-equation implementing changes in matrix velocity dependent on lithology and demonstrate the general applicability of refraction seismics to differentiate frozen and unfrozen low-porosity bedrock.

1 Introduction

Most polar and many mountainous regions of the earth are underlain by permafrost, making them especially sensitive to climate change (IPCC, 2007; Nogués-Bravo et al., 2007). Permafrost is a thermally defined phenomenon referring to ground that remains below 0 °C for at least two consecutive years (NRC-Permafrost-Subcommitee, 1988). Permafrost is not synonymous with perennially frozen underground due to freezing point depression resulting from solutes, pressure, pore diameter and pore material (Krautblatter et al., 2010; Lock, 2005). Ice develops in pores and cavities (Hallet et al., 1991) and affects the thermal, hydraulic and mechanical properties of the underground. Climate Change can degrade permafrost and, thus, alters permafrost distribution. In mountainous regions, rockwalls with degrading permafrost are considered to be a major hazard due to rockfall activity and slow rock deformation (Gruber and Haeberli, 2007; Krautblatter et al., 2012).

Surface-based geophysical methods represent a cost-effective approach for permafrost characterization (Harris et al., 2001). The application of geophysical methods has a long tradition in permafrost studies (Akimov et al., 1973; Barnes, 1965; Ferrians and Hobson, 1973; Scott et al., 1990). Hauck and Kneisel (2008a) and Kneisel et al. (2008) provide an overview about geophysical methods suitable for permafrost monitoring in high-mountain environments. In contrast to direct temperature measurements in boreholes, geophysical methods provide only indirect information about permafrost occurrence. On the other hand, geophysical methods are non-invasive, provide spatial 2-D/3-D information and are also applicable in instable fractured rock. Frozen ground changes the properties of underground materials, the degree of change depends on water content, pore size, pore water chemistry, sub-surface temperature and material pressure (Scott et al., 1990). In field applications, the most prominent geophysical parameters for the differentiation between frozen and unfrozen underground are electrical resistivity and compressional wave velocity (Hauck, 2001). Alpine rock cliffs in permafrost regions mostly consist of hard low-porosity rocks (< 10 %), according to Tiab and Donaldson's (2004) definition, and the applicability of electrical and seismic methods to these is yet unclear. While the relationship between electrical resistivity and frozen low-porosity bedrock has been investigated by Krautblatter et al. (2010), this article will focus on the applicability of p-wave refraction seismics to low-porosity bedrock.

The p-wave velocity of freezing rocks was investigated in the laboratory mostly using polar high-porosity (> 10 %) sedimentary rocks (Dzhurik and Leshchikov, 1973; King, 1977; Pandit and King, 1979; Pearson et al., 1986; Remy et al., 1994; Sondergeld and Rai, 2007; Timur, 1968). Only few studies included low-porosity (< 10 %) sedimentary rocks (Pearson et al., 1986; Timur, 1968), igneous rocks (Takeuchi and Simmons, 1973; Toksöz et al., 1976) and metamorphic rocks (Bonner et al., 2009). Early laboratory studies demonstrated compressional and shear wave velocity increases in freezing bedrock (King, 1977; Timur, 1968). Seismic velocities increase at sub-zero temperatures until they reach a plateau when most of the pores are frozen and the unfrozen water content is negligible (Pandit and King, 1979; Pearson et al., 1986). P-wave velocity of freezing rocks is controlled by the original water-filled porosity, i.e. the velocity corresponds to the changing proportion of frozen and unfrozen pore water content (King et al., 1988). In that sense, saline pore water increases the unfrozen pore water content at a given temperature (Anderson and Morgenstern, 1973; Tice et al., 1978) and flattens the otherwise sharp p-wave velocity increase when freezing (Pandit and King, 1979). Some authors observed hysteresis effects between ascending and descending temperature runs and assumed supercooling of the pore water during the descending temperature run as a reason (King, 1977; Nakano et al., 1972).

These findings have been transferred to field applications of p-wave velocity refraction seismics to various sedimentary landforms in polar environments (Bonner et al., 2009; Harris and Cook, 1986; King, 1984; Kurfurst and Hunter, 1977; Roethlisberger, 1961; Zimmerman and King, 1986) and to rock glaciers (Barsch, 1973; Hausmann et al., 2007; Ikeda, 2006; Musil et al., 2002), to bedrock (Hauck et al., 2004) and to talus slopes (Hilbich, 2010) in mountainous regions. Akimov et al. (1973) note the discrepancy between seismic laboratory and field investigations. Due to different ambient settings, the comparison of small-scale laboratory results to large-scale field applications is complicated. These include a high rate of cooling, a non-representation of the stressed state of material as found in field conditions, supercooling and the time required for transition into ice in laboratory studies.

Wyllie et al. (1956) developed a time-average equation

$$\frac{1}{v} = \frac{\Phi}{v_\mathrm{l}} + \frac{1-\Phi}{v_\mathrm{m}}, \tag{1}$$

where v is the measured velocity, v_l is the velocity of the liquid inside the pore space, v_m is the matrix velocity and Φ is the porosity, based on measurements of sandstone ($0.02 < \Phi < 0.32$) and limestone samples ($0.001 < \Phi < 0.18$). The time-average equation requires a relative uniform mineralogy, fluid saturation and high effective pressure (Mavko et al., 2009). To fulfil the seismic ray assumption of the time-average equation the wavelength should be small compared with typical pore and grain size, respectively, and the pores and grains should be arranged as homogenous layers perpendicular to seismic ray path (Mavko et al., 2009). Due to larger size and more heterogeneous distribution of vugular, i.e. secondary solution-related, pores in carbonate rocks, p-wave velocities of carbonate rocks show less dependency on porosity and the time-average equation underestimates the p-wave velocities (Wyllie et al., 1958). The two-phase model of Timur (1968) modified the Eq. (1) to frozen states,

$$\frac{1}{v} = \frac{\Phi}{v_\mathrm{i}} + \frac{1-\Phi}{v_\mathrm{m}} \tag{2}$$

where v_i is the velocity of ice in the pore space. Timur (1968) extended Eq. (2) to a three-phase time-average equation:

$$\frac{1}{v} = \frac{(1-S_\mathrm{i})\Phi}{v_\mathrm{l}} + \frac{S_\mathrm{i}\Phi}{v_\mathrm{i}} + \frac{1-\Phi}{v_\mathrm{m}} \tag{3}$$

with S_i is the relative fraction of pore space occupied by ice. Equation (2) and Eq. (3) were tested for sandstone ($0.13 < \Phi < 0.42$), carbonate ($0.15 < \Phi < 0.47$) and shale samples ($0.04 < \Phi < 0.10$). McGinnis et al. (1973) deduced that the relative p-wave velocity increases upon freezing Δv_p [%] versus porosity is

$$\Delta v_\mathrm{p} = \frac{\Phi - 0.0363}{0.0044} \tag{4}$$

based on a linear regression of Timur's (1968) measurements; a formula that implies that there are no p-wave velocity changes below 3.6 % porosity. This relation was only used as an interpretation tool for their field measurements and possesses no validity for low-porosity rocks. Hauck et al. (2011) extended Timur's (1968) equation to 4 phases and weighted the p-wave velocities of the components by their volumetric fractions:

$$\frac{1}{v} = \frac{f_\mathrm{l}}{v_\mathrm{l}} + \frac{f_\mathrm{m}}{v_\mathrm{m}} + \frac{f_\mathrm{i}}{v_\mathrm{i}} + \frac{f_\mathrm{a}}{v_\mathrm{a}} \tag{5}$$

$$f_\mathrm{l} + f_\mathrm{m} + f_\mathrm{i} + f_\mathrm{a} = 1 \text{ and } 0 \le f_\mathrm{l},\ f_\mathrm{m},\ f_\mathrm{i},\ f_\mathrm{a} \le 1 \tag{6}$$

where v_a is the velocity of air, f_l is the volumetric fraction of liquid water, f_r is the volumetric fraction of rock, f_i is the volumetric fraction of ice and f_a is the volumetric fraction of air. Carcione and Seriani (1998) give an overview about existing modelling of permafrost based on seismic velocities mostly for unconsolidated porous media (King et al., 1988; Leclaire et al., 1994; Zimmerman and King, 1986).

The influence of pressure on seismic velocities (Nur and Simmons, 1969) and porosity (Takeuchi and Simmons, 1973; Toksöz et al., 1976) is observed by many researchers (King, 1966; Wang, 2001). Two pressures can be distinguished, the confining or overburden pressure of the rock mass and the pore pressure of the fluid. These can reinforce or compete with each other, which is expressed by different values of n (Wang, 2001). The effective pressure (P_e) is

$$P_e = P_c - nP_p, \tag{7}$$

where P_c is the confining pressure, P_p is the pore pressure and $n \leq 1$. The net overburden pressure (P_d) is then described as

$$P_d = P_c - P_p. \tag{8}$$

Pores react to an increasing confining pressure according to their shape: spheroidal pores deform and become thinner while spherical pores decrease in volume (Takeuchi and Simmons, 1973; Toksöz et al., 1976). P-wave velocity will increase due to decreasing porosity if the confining pressure does not surpass the damage threshold and porosity increase due to microcracking (Eslami et al., 2010; Heap et al., 2010; Wassermann et al., 2009). In measurements with high confining pressures, the effect of pores is negligible but the effects of cracks become more important (Takeuchi and Simmons, 1973). In frozen rocks, the ice pressure effect is most pronounced for spheroidal "flat" pores or cracks (Toksöz et al., 1976).

Pore shape, cracks and fractures also determine seismic anisotropy next to anisotropic mineral components and textural-structural characteristics such as bedding and cleavage (Barton, 2007; Lo et al., 1986; Thomsen, 1986; Vernik and Nur, 1992; Wang, 2001). The two latter causes are referred to as intrinsic anisotropy and cannot decrease as a result of pressure (Barton, 2007; Lo et al., 1986; Thomsen, 1986). In contrast, "induced anisotropy" through pores, cracks and fractures corresponds to stress. Stress increase due to loading can preferentially close pre-existing microcracks perpendicular to stress direction and decreases anisotropy (Eslami et al., 2010; Heap et al., 2010; Wassermann et al., 2009). However, stress increase can also lead to preferential opening of axially orientated microcracks (Eslami et al., 2010) or microcrack generation due to threshold surpassing (Heap et al., 2010; Wassermann et al., 2009), which then enhances anisotropy. The anisotropy A is defined as

$$A = \frac{\upsilon_{max} - \upsilon_{min}}{\upsilon_{max}}, \tag{9}$$

where υ_{max} is the faster velocity of both compressional waves parallel and perpendicular to cleavage or bedding and υ_{min} is the slower velocity (Johnston and Christensen, 1995).

We postulate that p-wave velocity measurements in low-porosity rocks could become an important method for the monitoring of Alpine rock wall permafrost. This study aims at (1) measuring the p-wave velocity increases in low-porosity rocks, (2) evaluating the increase of matrix velocity due to ice pressure, (3) describing the alteration of seismic anisotropy due to changes of induced pore pressure and (4) incorporating this matrix velocity increase in the time-average equation.

2 Methodology

We tested 20 Alpine and 2 Arctic rock specimens between 1.8 and 25 kg sampled from several permafrost sites (see Table 1 for details). We used large rock specimens with a statistical distribution of > 100 fissures, cracks and cleavages in a sample to cope with natural bedrock heterogeneity (Akimov et al., 1973; Jaeger, 2009; Matsuoka and Murton, 2008). All samples were immersed in water under atmospheric conditions until full saturation indicated by a constant weight was achieved (W_s). The free saturation method resembles the field situation more closely than saturation under vacuum conditions (Krus, 1995; Sass, 2005) but probably includes air bubbles and can complicate the interpretation. After that, the samples are dried at 105 °C to a constant weight (W_d). The ratio of weight difference between saturated and dry weight is equal to moisture content in percentage by weight. This multiplied by the rock density is effective porosity Φ_{eff} and includes only hydraulically-linked pores (Sass, 2005). Rock density is derived from Wohlenberg (2012).

To distinguish quantitatively connected and unconnected pores will help the interpretation but necessary methods were not available. In an earlier study by Krautblatter (2009), six plan-parallel cylindrical plugs were prepared with diameter and length of 30 mm from six of the 22 samples used in this study and porosity values were measured using a gas compression/expansion method in a Micromeritics Multivolume Pycnomter 1305. These absolute porosity values are used to estimate the quality of the effective porosity values.

All 22 samples were immersed again for 48 h under atmospheric conditions and the saturated weight $W_{48\,h}$ was determined. To determine the moisture conditions we calculated the degree of saturation S_r

$$S_r = \frac{(W_{48\,h} - W_d)}{(W_s - W_d)}. \tag{10}$$

Subsequently, samples were loosely coated with plastic film to protect them against drying and were cooled in a range of 25 °C to −15 °C in a WEISS WK 180/40 high-accuracy climate chamber (Fig. 1). The cooling rate was first 7 °C h^{-1} until sudden p-wave velocity increase due to

Table 1. Rock samples, source, lithology, geologic description (fabric), porosity (Φ) and degree of saturation (S_r).

Sample	Location (Country)	Landform	Sort of sample	Lithology	Geological description (fabric)	Porosity Φ [%]	Porosity S_r	publ. data
A5	Steintaelli/Mattervalley (CH)	Rock wall	Q	pyritic paragneiss	metamorphic lamination	1.04 ± 0.14	0.99	1–4
H1	Matterhorn/Mattervalley (CH)	Rock wall	S	gneiss	metamorphic lamination	0.93 ± 0.12	1.00	5–6
X5	Zastler/Black Forest (D)	Scree slope	S	gneiss	metamorphic lamination	0.95 ± 0.12	1.00	7
				gneiss		*0.97 ± 0.04*		
X2	Pasterze/Grossglockner (A)	Glacier forefield	S	serpentine	mixed fabric directions	1.27 ± 0.16	1.00	8
H2	Matterhorn/Mattervalley (CH)	Rock wall	S	amphibolite	mixed fabric directions	1.31 ± 0.08	0.96	5–6
				other metamorphic rocks		*1.14 ± 0.13*		
S1	Steintaelli/Mattervalley (CH)	Rock wall	Q	schisty quartz slate	planar slaty cleavage	2.40 ± 0.12	0.96	1–4
S4	Steintaelli/Mattervalley (CH)	Rock wall	Q	schisty quartz slate	planar slaty cleavage	1.94 ± 0.10	0.94	1–4
S3	Steintaelli/Mattervalley (CH)	Rock wall	Q	quartz slate	planar schistosity	1.49 ± 0.08	0.98	1–4
X8	Murtel/Upper Engadin (CH)	Rock glacier	S	greenschist	planar schistosity	1.86 ± 0.13	0.97	9–10
A22	Bliggspitze/Kaunervalley (A)	Rock wall	Q	mica schist	planar schistosity	1.56 ± 0.11	1.00	11
X13	Kitzsteinhorn (A)	Rock wall	S	mica schist	planar schistosity	0.83 ± 0.06	0.91	12
D2	Muragl/Upper Engadin (CH)	Rock glacier	S	mica schist	planar schistosity	1.04 ± 0.07	1.00	9–10, 13
C1	Corvatsch/Upper Engadin (CH)	Rock wall	Q	migmatic schist	planar schistosity	2.76 ± 0.27	0.94	14
C2	Corvatsch/Upper Engadin (CH)	Rock wall	Q	migmatic schist	planar schistosity	1.56 ± 0.15	0.99	14
				schists		*1.48 ± 0.50*		
M1	Aiguille du Midi (F)	Rock wall	Q	granite	no pronounced fabric	1.31 ± 0.07	1.00	15–16
X9	Gemsstock (CH)	Rock wall	Q	granodiorite	no pronounced fabric	2.25 ± 0.05	0.99	17
				plutonic rocks		*1.43 ± 0.55*		
X6	Präg/Black Forest (D)	Scree slope	S	andesite	no pronounced fabric	3.03 ± 0.35	1.00	7
X7	Präg/Black Forest (D)	Scree slope	S	andesite	no pronounced fabric	3.45 ± 0.40	1.00	7
				volcanic rocks		*3.24 ± 0.21*		
L1	Longyeardalen/Svalbard (N)	Rock wall	Q	Endalen Sandstone	no pronounced fabric between bedding planes (sample size)	5.21 ± 0.96	1.00	18
L2	Longyeardalen/Svalbard (N)	Talus slope	S	Endalen Sandstone	no pronounced fabric between bedding planes (sample size)	6.03 ± 1.11	1.00	18
				clastic rocks		*5.62 ± 0.41*		
A8	Zugspitze/Wettersteingebirge (D/A)	Rock wall	Q	Wetterstein Dolomite	no pronounced fabric between bedding planes (sample size)	1.91 ± 0.16	1.00	19–20
K1	Saumur/Loire Valley (F)	Sedimentary bassin	Q	Tuffeau Limestone	no pronounced fabric between bedding planes (sample size)	45.16 ± 5.96	0.95	21–23
				carbonate rocks		*23.54 ± 21.63*		

Q = quarried out of rock wall , S = picked from the surface; 1 = Krautblatter and Hauck (2007), 2 = Krautblatter (2008), 3 = Krautblatter (2009), 4 = Krautblatter (2010), 5 = Hasler et al. (2011), 6 = Hasler et al. (2012), 7 = Hauck and Kneisel (2008b), 8 = Geilhausen et al. (2012), 9 = Maurer and Hauck (2007), 10 = Hauck et al. (2011), 11 = Krautblatter et al. (2009), 12 = Hartmeyer et al. (2012), 13 = Musil et al. (2002), 14 = Gubler et al. (2011), 15 = Ravanel and Deline (2010), 16 = Deline et al. (2009), 17 = Kenner et al. (2011), 18 = Siewert et al. (2012), 19 = Krautblatter et al. (2010), 20 = Verleysdonk et al. (2011), 21 = Murton et al. (2000), 22 = Murton et al. (2001), 23 = Murton et al. (2006).

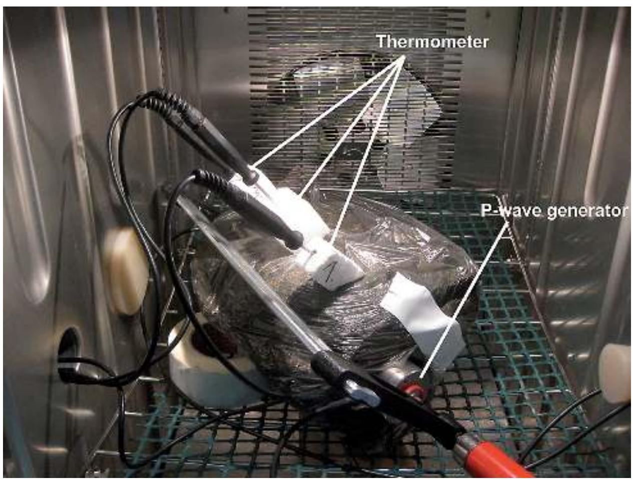

Fig. 1. Laboratory measurement set up of a p-wave velocity measurement of a schisty quartz slate sample (S1) in parallel direction to cleavage. Drilled into the rock sample are three thermometers to monitor rock temperature.

freezing and was then decreased to $6\,°\mathrm{C\,h^{-1}}$ (Matsuoka, 1990). Ventilation was applied to avoid thermal layering. Two to three calibrated 0.03 °C-accuracy thermometers were drilled into the rock samples to depths between 3 and 10 cm and a spacing of approximately up to 10 cm depending on sample size. Rock temperature at different depths and spacings were measured to account for temperature homogeneity in the sample (Krautblatter et al., 2010). The p-wave generator Geotron USG 40 and the receiver were placed on flattened or cut opposite sides of the cuboid samples. The wavelength of the generator was 20 kHz to fulfill requirements of the time-average equation; dispersion of p-wave velocities due to wavelengths are negligible (Winkler, 1983). The travel time of the p-wave was picked using a Fluke ScopeMeter 192B with an accuracy of $1–2 \times 10^{-6}$ s. The internal deviation induced by the measurement procedure was assessed by conducting five subsequent travel time measurements. To account for the anisotropy of the rock samples, we measured p-wave velocities in the same sample in the direction of cleavage/bedding and perpendicular to the cleavage/bedding direction. The matrix velocity v_m is calculated by solving Eq. (2). The velocity of the material in the pore space v_i is $1570\,\mathrm{m\,s^{-1}}$ for water in the unfrozen status and $3310\,\mathrm{m\,s^{-1}}$ for ice (Timur, 1968), we replaced porosity with effective porosity in the calculation. Matrix velocity is calculated for frozen (−15 °C) and unfrozen status (mean value of $v > 0$ °C) both for parallel and perpendicular to cleavage/bedding measurements according to

$$v_m = \frac{1-\Phi}{\frac{1}{v} - \frac{\Phi}{v_i}}. \qquad (11)$$

The change of matrix velocity Δv_{m} due to freezing is calculated according to

$$\Delta v_{\mathrm{m}} = \frac{v_{\mathrm{mf}} - v_{\mathrm{ms}}}{v_{\mathrm{ms}}}, \tag{12}$$

where v_{mf} is the matrix velocity in the frozen status and v_{ms} is the matrix velocity in the saturated status. The change of anisotropy ΔA due to freezing will be calculated according to

$$\Delta A = A_{\mathrm{s}} - A_{\mathrm{f}}, \tag{13}$$

where A_{s} is the anisotropy after 48 h saturation and A_{f} is the anisotropy for frozen status.

3 Results

Tables 1 and 2 give an overview about measured rock samples and their rock properties and seismic velocities. Figure 2 represents the evolution of p-wave velocities dependent on rock temperature of six selected rock samples from six different lithologies.

3.1 Porosities and degree of saturation

The absolute (vacuum) porosity values comprehending connected and non-connected porosity measured for 6 samples (A5, X2, S1, S3, X9, A8) by Krautblatter (2009) are compared with the effective (atmospheric pressure) porosity values comprehending only connected porosity. The absolute porosity (2.60 ± 0.21 %) is on average 30 % higher than the effective porosity (1.72 ± 0.12 %), only in slate samples both were equivalent.

Rock samples are classified according to their lithology into three metamorphic, two igneous and two sedimentary rock clusters. Absolute deviations of porosity within the clusters are less than 1 % except for carbonate rock samples. After 48 h saturation, gneiss, plutonic rocks, volcanic rocks and clastic rocks show mean S_{r} of 1.00; other metamorphic rocks (mean $S_{\mathrm{r}} = 0.98$), schists (mean $S_{\mathrm{r}} = 0{,}97$) and carbonate rocks (mean $S_{\mathrm{r}} = 0.98$) are not fully saturated, but all could possibly develop cryostatic pressure on the volumetric expansion of ice in more than 91 % saturated pores (Walder and Hallet, 1986).

3.2 P-wave velocities of frozen rock

P-wave velocity increases significantly as a result of freezing in all 22 samples. Supercooling causes hysteresis effects resulting in sudden latent heat release and rock temperature increase observed in 16 of 22 samples and indicated as p-wave velocity hysteresis of three rock samples (A5, X8, L2) in Fig. 2. Parallel to cleavage/bedding, p-wave velocity increase is highest in sedimentary (carbonate and clastic) rocks, followed by magmatic (volcanic and plutonic) rocks and lowest in metamorphic rocks (schists, other metamorphic rocks and gneiss) (Fig. 3a). The order remains the same perpendicular to cleavage/bedding except for schists (Fig. 3b).

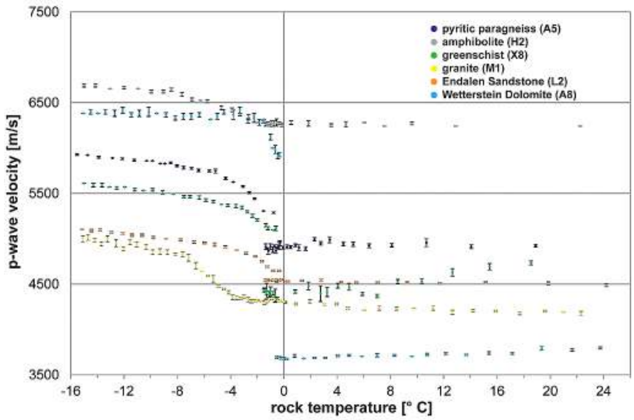

Fig. 2. P-wave velocity of several rock samples measures parallel to cleavage or bedding plotted against rock temperature; error bars indicate mean deviation of p-wave velocities.

3.3 Porosity dependent change in p-wave velocities

Existing time-average models assume a dependence of p-wave velocity increase on porosity. We plotted the increase of p-wave velocity due to freezing measured and calculated with Eq. (2) against the mean effective porosity (Fig. 4a and b). We excluded the carbonate rocks due to their vugular pores and the constrained applicability of the time-average equation (Wyllie et al., 1958). All measured p-wave velocity increases are much higher than calculated according to Eq. (2), expected as a result of phase transition from water ($1570\,\mathrm{m\,s^{-1}}$) to ice ($3310\,\mathrm{m\,s^{-1}}$) only. Parallel to cleavage or bedding, the offset between measured and calculated results is increasing from gneiss ($296 \pm 205\,\mathrm{m\,s^{-1}}$), schists ($642 \pm 314\,\mathrm{m\,s^{-1}}$), other metamorphic rocks ($685 \pm 200\,\mathrm{m\,s^{-1}}$), plutonic rocks ($686 \pm 0\,\mathrm{m\,s^{-1}}$), clastic rocks ($815 \pm 683\,\mathrm{m\,s^{-1}}$), to volcanic rocks ($1158 \pm 278\,\mathrm{m\,s^{-1}}$). Perpendicular to cleavage or bedding, the offset increases from other metamorphic rocks ($414 \pm 210\,\mathrm{m\,s^{-1}}$), gneiss ($467 \pm 108\,\mathrm{m\,s^{-1}}$), volcanic rocks ($529 \pm 183\,\mathrm{m\,s^{-1}}$), plutonic rocks ($561 \pm 41\,\mathrm{m\,s^{-1}}$), clastic rocks ($626 \pm 474\,\mathrm{m\,s^{-1}}$) to schists ($1368 \pm 695\,\mathrm{m\,s^{-1}}$).

3.4 Matrix velocity

The increase in p-wave velocity is too high to be solely explained by changes of the p-wave velocity in the pore infill as is suggested by Timur (1968). Here, the additional change in p-wave velocity is explained by the increase in matrix velocity as shown in Eq. (11) and Eq. (12). All measured rock samples show significant matrix velocity increases v_{m} (see Table 2) due to freezing except one gneiss sample (X5). Timur

Table 2. Rock samples classified into lithological groups and seismic properties. The table shows p-wave velocity of a saturated unfrozen (v_{ps}) and a frozen (v_{pf}) sample, p-wave velocity increase due to freezing (Δv_p), matrix velocity of a saturated unfrozen (v_{ms}) and a frozen (v_{mf}) sample, matrix velocity increase due to freezing (Δv_m), anisotropy of a saturated (A_s) and a frozen (A_f) sample and the decrease of anisotropy due to freezing (ΔA).

Sample/	P-wave velocity						Matrix Velocity						Anisotropy		
Rock	parallel			perpendicular			parallel			perpendicular					
class	V_{ps} [m s^{-1}]	V_{pf} [m s^{-1}]	ΔV_p [m s^{-1}]	V_{ps} [m s^{-1}]	V_{pf} [m s^{-1}]	ΔV_p [m s^{-1}]	V_{ms} [m s^{-1}]	V_{mf} [m s^{-1}]	ΔV_m [m s^{-1}]	V_{ms} [m s^{-1}]	V_{mf} [m s^{-1}]	ΔV_m [m s^{-1}]	A_s [%]	A_f [%]	ΔA [%]
A5	6261	6689	428	4774	5474	700	6479	6749	270	4869	5481	612	23.75	18.16	5.59
H1	5401	6099	698	4933	5399	466	5529	6148	619	5034	5432	398	8.67	11.48	−2.81
X5	5699	5826	127	5007	5467	460	5858	5850	−8	5110	5480	370	12.14	6.16	5.98
gneiss			*418 ± 194*			*542 ± 105*			*294 ± 217*			*460 ± 101*			*2.92*
X2	5275	5873	598	4381	4672	291	5432	5923	491	4488	4687	199	16.95	20.45	−3.50
H2	4934	5929	995	4611	5356	745	5080	5992	912	4760	5401	641	6.55	9.66	−3.12
other metamorphic rocks			*797 ± 199*			*518 ± 227*			*702 ± 211*			*420 ± 221*			*−3.31*
S1	5249	5805*	556*	1953	4373*	2420*	5564	5906*	342*	1969	4400*	2431*	62.79	24.67*	38.12
S4	5236	5942*	706*	1667	4425*	2758*	5506	6037*	531*	1667	4455*	2788*	68.16	25.53*	42.63
S3	5116	6096	980	2615	3636	1021	5294	6165	871	2655	3631	976	48.89	40.35	8.53
X8	4682	5480	798	4504	5612	1108	4869	5540	671	4683	5687	1004	3.80	2.35	1.45
A22	4329	5833	1504	3882	5274	1392	4454	5904	1450	3942	5303	1361	10.33	9.58	0.74
X13	5740	6224	484	5263	5786	523	5868	6270	402	5395	5799	404	8.31	7.04	1.27
D2	5018	5373	355	4836	5355	519	5140	5408	340	4943	5352	409	3.63	0.34	3.29
C1	4030	5293	1263	2189	4356	2167	4249	5385	1136	2228	4395	2167	45.68	17.70	27.98
C2	5502	5978*	476*	1664	2595*	931*	5735	6051*	316*	1640	2579*	939*	69.76	56.59*	13.17
schists			*791 ± 307*			*1427 ± 681*			*673 ± 319*			*1387 ± 717*			*15.24*
M1	4228	5000	772	3583	4178	595	4332	5011	679	3663	4180	517	15.26	16.44	−1.18
X9	5191	6078	887	4039	4759	720	5471	6194	723	4181	4808	627	22.19	21.70	0.49
plutonic rocks			*830 ± 58*			*658 ± 63*			*701 ± 22*			*572 ± 55*			*−0.35*
X6	4345	6000	1655	4935	5538	603	4618	6129	1511	5286	5657	371	11.96	7.70	4.26
X7	4426	5541	1115	4317	5248	931	4730	5678	948	4597	5360	763	2.46	5.29	−2.83
volcanic rocks			*1385 ± 270*			*767 ± 164*			*1230 ± 282*			*567 ± 196*			*0.72*
L1	3422	5130	1708	5363	4904	1341	3652	5290	1638	3835	5031	1196	3.96	4.41	−0.45
L2	4521	5105	584	3989	4502	513	5139	5290	151	4440	4608	168	11.77	11.81	−0.04
clastic rocks			*1146 ± 562*			*927 ± 414*			*895 ± 744*			*682 ± 514*			*−0.25*
A8	3723	6383	2660	1879	6068	4189	3838	6500	2662	1864	6161	4297	49.53	4.93	44.59
K1	2247	4167	1920	2014	4211	2197	3566	5332	1766	2647	5467	2820	10.37	1.04	9.32
carbonate rocks			*2290 ± 370*			*3193 ± 996*									*26.96*

* indicates lowest sample temperatures above −10 °C.

(1968) expected no matrix velocity increase due to freezing. Figure 4 shows that Timur's Eq. (2) underestimates the measured p-wave velocity significantly.

3.5 Anisotropy

Anisotropy A is calculated according to Eq. (9) for conditions after 48 h saturation (A_s) and frozen conditions at $-15\,°\mathrm{C}$ (A_f). Induced anisotropy due to pores, cracks and fractures can be reduced through pressure (Barton, 2007; Wang, 2001). Anisotropy alteration ΔA is calculated according to Eq. (13). In our experimental setup, pore ice pressure reduces induced anisotropy due to the closure of pores, cracks and fractures, while the confining (atmospheric) pressure remains constant. The pore pressure changes due to the phase transition from water to ice in saturated pores. Ice develops pressure through volumetric expansion and ice segregation (Matsuoka, 1990; Matsuoka and Murton, 2008). 15 of 22 samples show an anisotropy reduction due to freezing (1–45 %), which is especially pronounced in slates, schists and carbonates. Seven samples show negligible ($n = 3$, < 1.50 %) or small ($n = 4$, ≤ 3.50 %) increases in anisotropy when freezing. Three samples (L1, L2, M1) show a low anisotropy increase, the anisotropy of four other samples (H1, H2, X2, X7) increases slightly.

4 Discussion

4.1 Model setup and representativeness

Previous studies (McGinnis et al., 1973; Timur, 1968) explained p-wave velocity increases exclusively as an effect of porosity and infill. We postulate, that these models apply well for soft high-porosity rocks but cannot be transferred to hard low-porosity rocks. This is due to the fact that the effects of freezing are determined by multiple factors including (i) porosity but also (ii) the pore form and the degree of fissuring and (iii) ice pressure development. Here, we try to derive a straightforward model that explains the effects of freezing in low-porosity rocks on p-wave velocity.

(i) We have tested 7 clusters or 22 specimens of low-porosity rocks. These indicate p-wave velocity increases from $518 \pm 227\,\mathrm{m\,s^{-1}}$ (other metamorphic rocks), $542 \pm 105\,\mathrm{m\,s^{-1}}$ (gneiss), $658 \pm 63\,\mathrm{m\,s^{-1}}$ (plutonic rocks), $767 \pm 164\,\mathrm{m\,s^{-1}}$ (volcanic rocks), $927 \pm 414\,\mathrm{m\,s^{-1}}$ (clastic rocks), $1427 \pm 681\,\mathrm{m\,s^{-1}}$ (schists) to $3193 \pm 996\,\mathrm{m\,s^{-1}}$ (carbonate rocks) perpendicular to cleavage or bedding. Timur's (1968) model would, respectively, anticipate p-wave velocity changes from $104 \pm 17\,\mathrm{m\,s^{-1}}$ (other metamorphic rocks), $75 \pm 2\,\mathrm{m\,s^{-1}}$ (gneiss), $96 \pm 21\,\mathrm{m\,s^{-1}}$ (plutonic rocks), $238 \pm 19\,\mathrm{m\,s^{-1}}$ (volcanic rocks), $301 \pm 60\,\mathrm{m\,s^{-1}}$

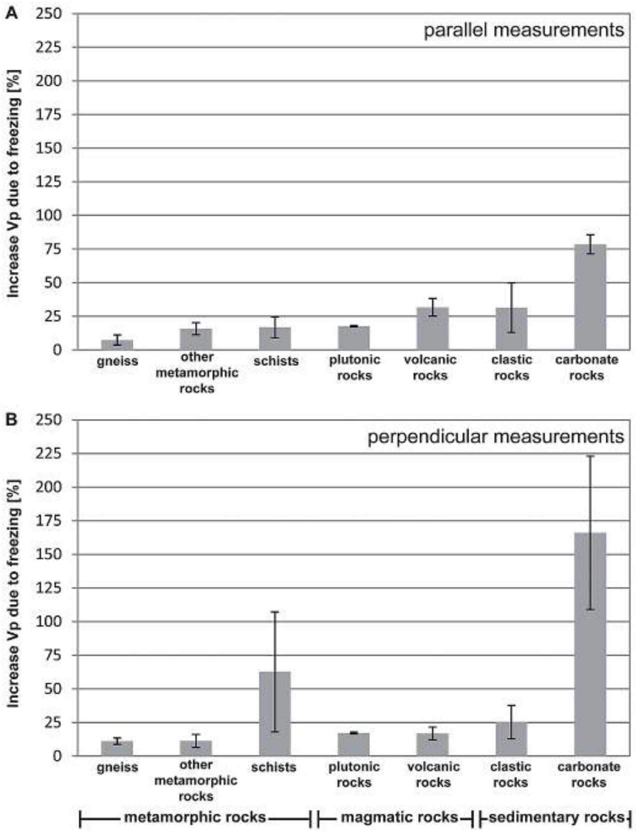

Fig. 3. P-wave velocity increase of samples in percent for rock groups classified based on lithology; **(A)** parallel to cleavage/bedding and **(B)** perpendicular to cleavage/bedding; error bars indicate mean deviation.

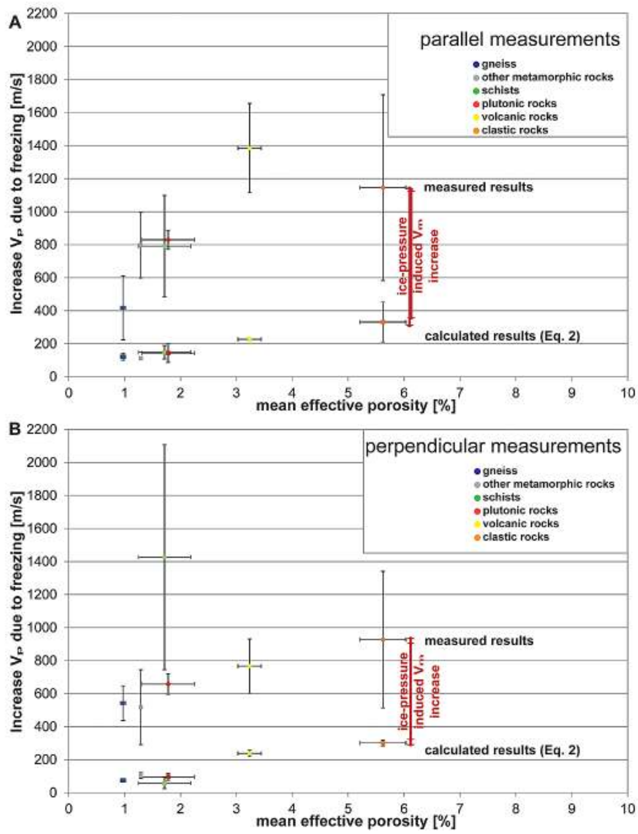

Fig. 4. P-wave velocity (v_p) increase due to freezing plotted against mean effective porosities for six different rock groups. P-wave velocity increases **(A)** parallel to cleavage or bedding and **(B)** perpendicular to cleavage/bedding, the dots are measured values and the quadrats are values calculated using Eq. (2).

(clastic rocks) to $58 \pm 34\,\mathrm{m\,s^{-1}}$ (schists) and underestimates strongly p-wave velocity increases in low-porosity bedrock (Fig. 4b). Due to vugular pores, the time-average equation and Eq. (2) are not applicable to carbonate rocks (Wyllie et al., 1958) and we excluded them from further calculations. The offset between measured velocities and calculated velocities shows that porosity is not the dominant determinant of p-wave velocity changes in low-porosity bedrock. Calculations of p-wave velocities parallel to cleavage or bedding reflect this offset trend but are violating the seismic ray assumptions of the time-average equation and should be used with caution for parallel velocities.

(ii) Pore form is among the most important factors for seismic properties (Nur and Simmons, 1969; Toksöz et al., 1976; Wang, 2001) and the most difficult one to quantify (Wang, 2001). Pore form determines pressure susceptibility (Takeuchi and Simmons, 1973; Toksöz et al., 1976) and ice effects (Toksöz et al., 1976) while pore linkage affects the saturation. Water-saturated porosity controls p-wave velocity (King, 1977; King et al., 1988) and frost weathering (Matsuoka, 1990; Matsuoka and Murton, 2008; Sass, 2005). We assume no influence of salinity due to low solubility of rock minerals in the used specimens (Krautblatter, 2009). Hydraulically linked porosity is best described by effective porosity (Sass, 2005) and we replace porosity in Eq. (2) with effective porosity. In future studies, the pore form could be assessed by porosimetric analyses and, thus, the differentiation of connected and non-connected porosity would facilitate a quantitative interpretation. However, calculating matrix velocity with absolute porosity values would change matrix velocity only by $2 \pm 2\,\%$, which is well below the accuracy within the clusters. The weathering history determines the enlargement of pores, fissures and fractures in permafrost and non-permafrost samples, and we assume that the long periglacial weathering history of high-alpine and arctic samples affects pore shape and connectivity. Previous mentioned studies mostly used high-porosity arctic specimens from Mesozoic sedimentary rocks and frost susceptibility in these low-strength rocks operates at a millimeter- to centimeter-scale (Matsuoka and Murton, 2008). We choose decimeter-large rock samples from several Alpine and one Arctic permafrost sites instead of standard bore cores. These are derived from the surface or quarried out of rock walls, are affected by permafrost in their history, include hundreds of micro-fissures, and represent the natural texture of permafrost-affected bedrock. This reflects that properties like pore distribution, texture, fissures and fractures provide the space and determine the effects of confined ice growth in hard rock samples (Matsuoka and Murton, 2008). In hard rocks, volumetric expansion and ice segregation is restricted by the rigid matrix and ice growth in pores and fissures causes high levels of stress inside the samples.

(iii) The variation of confining pressure related to rock overburden is a long-lasting process on a millennium scale, whereas pore pressure changes steadily (Matsuoka and Murton, 2008). Frequent daily freeze–thaw cycles reach a depth of approximately 30 cm (Matsuoka and Murton, 2008) while annual cycles often reach up to 5 m and more (Matsuoka et al., 1998). In our experiment the change in matrix velocity in combination with reduced anisotropy points towards "induced anisotropy" (Wang, 2001) in pores that reflects intrinsic stress generation. The pore pressure in the connected pores presumably increases due to ice stress applied on the matrix and probably closes non-connected porosity embedded in the matrix which results in decreasing anisotropy. A surpassing damage threshold or opening of microcracks could explain anisotropy increase. The pore pressure can be generated by the ice pressure building (Matsuoka, 1990; Vlahou and Worster, 2010) due to volumetric expansion of in situ water (Hall et al., 2002; Matsuoka and Murton, 2008) and ice segregation (Hallet, 2006; Murton et al., 2006; Walder and Hallet, 1985). In the laboratory, any open system allows water migration and enables ice segregation while closed systems with water-saturated samples favour volumetric expansion (Matsuoka, 1990). Our experimental setup is a quasi-closed system; water is only in situ available due to saturation and ice can leave through pores and joints. Due to 48 h saturation, the degree of saturation reaches at least 0.91 in all samples and the threshold for frost cracking as a result of volumetric expansion is fulfilled (Walder and Hallet, 1986). According to Sass (2005) and Matsuoka (1990) our quasi-closed system and fully saturated samples could be a good analogue to natural conditions.

Cooling rates of $6\,^{\circ}\mathrm{C\,h^{-1}}$ have been used by Matsuoka (1990) before and produce high expansion and freezing strain. Sass (2005) assumes high saturation of alpine rocks below the upper 10 cm. This is due to the fact that ice pressure is relaxed through ice deformation and ice expansion into free spaces (Tharp, 1987), ice extrusion (Davidson and Nye, 1985) and the contraction of samples was observed in the long-term due to ice creep (Matsuoka, 1990). In our system, samples cool from all outer faces which presumably act to seal the sample with ice. On the other hand, ice segregation along temperature gradients in fissured natural bedrock will cause suction up to several MPa (Murton et al., 2006; Walder and Hallet, 1985) and ice growth, and presumably cause a persistent elevated level of cryostatic stress similar to our laboratory setup.

4.2 A time-average model for low-porosity rock

Figure 4a and b show an offset which is not explainable by Eq. (2). This offset is induced by ice pressure. The way ice pressure is effective depends on the pore form of connected and non-connected pores. A quantitative analysis needs to distinguish between connected and non-connected pores. We use lithology as a proxy for pore form in our model and we assume an elevated level of stress in cryostatic systems. The pressure-induced variable m depends on lithology and is introduced as an extension of Eq. (2):

$$\frac{1}{v} = \frac{\Phi}{v_{\mathrm{i}}} + \frac{1-\Phi}{v_{\mathrm{m}}} \times \frac{1}{m} \tag{14}$$

where

$$m = 1 + \Delta v_{\mathrm{m}}; \tag{15}$$

Δv_{m} is the increase of matrix velocity empirically derived from our measurements. These general conclusions referenced by rock type are preliminary and should be applied with caution since we used a restricted number of samples. For our rock samples, we propose values of m of 1.09 ± 0.02 for gneiss, 1.09 ± 0.05 for other metamorphic rocks, 1.62 ± 0.45 for schists, 1.15 ± 0.00 for plutonic rocks, 1.12 ± 0.05 for volcanic rocks and 1.17 ± 0.13 for clastic rocks or, alternatively a general m of 1.34 ± 0.31 (Table 2). The use of Eq. (14) enhances to differentiate between frozen and unfrozen status of low-porosity rocks and can facilitate interpretation of field data.

5 Conclusions

Here, we propose to incorporate the physical concept of freezing in confined space into empirical mixing rules of p-wave velocities and present data (1) of p-wave measurements of 22 different alpine rocks, (2) evaluate the influence of ice pressure on seismic velocities, (3) determine anisotropic decrease due to ice pressure and (4) extend Timur's (1968) 2-phase model for alpine rocks:

(1) All tested rock samples show a p-wave velocity increase dependent on lithology due to freezing. P-wave velocity increases from $418 \pm 194\,\mathrm{m\,s^{-1}}$ for gneiss to $2290 \pm 370\,\mathrm{m\,s^{-1}}$ for carbonate rocks parallel to

cleavage/bedding; perpendicular measurements show an acceleration ranging from $518 \pm 105\,\mathrm{m\,s^{-1}}$ for other metamorphic rocks to $3193 \pm 996\,\mathrm{m\,s^{-1}}$ for carbonate rocks.

(2) P-wave velocity increases due to freezing are dominated by an increase of the velocity of the rock matrix while changes in pore-infill velocities are insignificant. Matrix velocity increases perpendicular to cleavage/bedding from $420 \pm 221\,\mathrm{m\,s^{-1}}$ for other metamorphic rocks to $1387 \pm 717\,\mathrm{m\,s^{-1}}$ for schists; parallel measurements reflect the matrix velocity increases perpendicular to cleavage but should be treated with caution.

(3) Anisotropy decreases by up to 45 % as a result of crack closure due to ice pressure in 15 of 22 rock samples. This effect is observed especially in all samples containing planar slaty cleavage or planar schistosity.

(4) We developed a novel time-average equation based on Timur's (1968) 2-phase equation with a lithology dependent variable to increase the matrix velocity responding to developing ice pressure while freezing.

This study provides the physical basis for the applicability of refraction seismics in low-porosity permafrost rocks. Due to their rigidity low-porosity bedrock cannot expand freely in response to ice pressure and, thus, matrix velocity increases. P-wave velocity increases predominantly as a result of ice pressure and to a lesser extent as a result of the higher velocity of ice than water in pores. The extension of the time average equation provides a more realistic calculation of the rock velocity and facilitates the interpretation of field data and possible permafrost distribution in alpine rock walls.

Acknowledgements. The authors thank G. Nover, J. Ritter and W. Scherer for equipment support to enable this study. Thanks to D. Amitrano and the anonymous reviewer for their extensive remarks and suggestions that helped a lot to improve the final paper. Also thanks to D. Funk for critical discussions, S. Verleysdonk for measurements, C. Hauck, C. Hilbich, L. Ravanel, A. Hasler, M. Siewert and P. Deline and M. Geilhausen for providing samples and all other involved persons.

Edited by: S. Gruber

References

Akimov, A. T., Dostovalov, B. N., and Yakupov, V. S.: Geophysical methods of studying permafrost, 2nd International Conference on Permafrost, USSR Contribution, Yakutsk, USSR, 767–777, 1973.

Anderson, D. M. and Morgenstern, N. R.: Physics, chemistry, and mechanics of frozen ground: A review, 2nd International Conference on Permafrost, Northamerican Contribution, Yakutsk, USSR, 257–288, 1973.

Barnes, D. F.: Geophysical methods for delineating permafrost, 1st International Conference on Permafrost, LaFayette, Indiana, 1963, 349–355, 1965.

Barsch, D.: Refraktionsseismische Bestimmung der Obergrenze des gefrorenen Schuttkörpers in verschiedenen Blockgletschern Graubündens, Schweizer Alpen, Zeitschrift für Gletscherkunde und Glazialgeologie, 9, 143–167, 1973.

Barton, N.: Rock quality, seismic velocity, attenuation and anisotropy, Routledge, London, Leiden, New York, 756 pp., 2007.

Bonner, J. L., Leidig, M. R., Sammis, C., and Martin, R. J.: Explosion Coupling in Frozen and Unfrozen Rock: Experimental Data Collection and Analysis, B. Seismol. Soc. Am., 99, 830–851, 2009.

Carcione, J. M. and Seriani, G.: Seismic and ultrasonic velocities in permafrost, Geophys. Prospec., 46, 441–454, doi:10.1046/j.1365-2478.1998.1000333.x, 1998.

Davidson, G. P. and Nye, J. F.: A Photoelastic Study of Ice Pressure in Rock Cracks, Cold Reg. Sci. Technol., 11, 141–153, 1985.

Deline, P., Coviello, V., Cremonese, E., Gruber, S., Krautblatter, M., Jaillet, S., Malet, E., Morra di Cella, U., Noetzli, J., Ravanel, L., Pogliotti, P., and Verleysdonk, S.: L'Aiguille du Midi (massif du Mont Blanc): un site remarquable pour l'étude du permafrost des parois d'altitude, Collection EDYTEM, Cahiers de Géographie, 8, 2009.

Dzhurik, V. and Leshchikov, F. N.: Experimental investigations of seismic properties of frozen soils, 2nd International Conference on Permafrost, USSR Contribution, Yakutsk, USSR, 485–488, 1973.

Eslami, J., Grgic, D., and Hoxha, D.: Estimation of the damage of a porous limestone from continuous (P- and S-) wave velocity measurements under uniaxial loading and different hydrous conditions, Geophys. J. Int., 183, 1362–1375, doi:10.1111/j.1365-246X.2010.04801.x, 2010.

Ferrians, O. J. and Hobson, G. D.: Mapping and predicting permafrost in North America: A review, 1963–1973, 2nd International Conference on Permafrost. Northamerican Contribution, Yakutsk, USSR, 1973, 479–498, 1973.

Geilhausen, M., Otto, J. C., and Schrott, L.: Spatial distribution of sediment storage types in two glacier landsystems (Pasterze & Obersulzbachkees, Hohe Tauern, Austria), J. Maps, 8, 242–259, doi:10.1080/17445647.2012.708540, 2012.

Gruber, S. and Haeberli, W.: Permafrost in steep bedrock slopes and its temperature-related destabilization following climate change, J. Geophys. Res.-Earth, 112, F02S18, doi:10.1029/2006JF000547, 2007.

Gubler, S., Fiddes, J., Keller, M., and Gruber, S.: Scale-dependent measurement and analysis of ground surface temperature variability in alpine terrain, The Cryosphere, 5, 431–443, doi:10.5194/tc-5-431-2011, 2011.

Hall, K., Thorn, C. E., Matsuoka, N., and Prick, A.: Weathering in cold regions: some thoughts and perspectives, Prog. Phys. Geog., 26, 577–603, 2002.

Hallet, B.: Geology – Why do freezing rocks break?, Science, 314, 1092–1093, 2006.

Hallet, B., Walder, J. S., and Stubbs, C. W.: Weathering by segregation ice growth in microcracks at sustained sub-zero temperatures: verification from an experimental study using acoustic emissions, Permafrost Periglac., 2, 283–300, doi:10.1002/ppp.3430020404, 1991.

Harris, C. and Cook, J. D.: The detection of high altitude permafrost in Jotunheimen, Norway using seismic refraction rechniques: an assessment, Arctic Alpine Res., 18, 19–26, 1986.

Harris, C., Davies, M. C. R., and Etzelmüller, B.: The assessment of potential geotechnical hazards associated with mountain permafrost in a warming global climate, Permafrost Periglac., 12, 145–156, 2001.

Hartmeyer, I., Keuschnig, M., and Schrott, L.: Long-term monitoring of permafrost-affected rock faces – A scale-oriented approach for the investigation of ground thermal conditions in alpine terrain, Kitzsteinhorn, Austria, Austrian J. Earth Sci., submitted, 2012.

Hasler, A., Gruber, S., and Haeberli, W.: Temperature variability and offset in steep alpine rock and ice faces, The Cryosphere, 5, 977–988, doi:10.5194/tc-5-977-2011, 2011.

Hasler, A., Gruber, S., and Beutel, J.: Kinematics of steep bedrock permafrost, J. Geophy. Res.-Sol. Ea., 117, F01016, doi:10.1029/2011jf001981, 2012.

Hauck, C.: Geophysical methods for detecting permafrost in high mountains, 171, ETH Zurich, Zurich, 1–204, 2001.

Hauck, C. and Kneisel, C.: Applied Geophysics in Periglacial Environments, University Press, Cambridge, 240 pp., 2008a.

Hauck, C. and Kneisel, C.: Quantifying the ice content in low-altitude scree slopes using geophysical methods, in: Applied Geophysics in Periglacial Environments, edited by: Hauck, C. and Kneisel, C., University Press, Cambridge, 153–164, 2008b.

Hauck, C., Isaksen, K., Vonder Mühll, D., and Sollid, J. L.: Geophysical surveys designed to delineate the altitudinal limit of mountain permafrost: an example from Jotunheimen, Norway, Permafrost Periglac., 15, 191–205, 2004.

Hauck, C., Böttcher, M., and Maurer, H.: A new model for estimating subsurface ice content based on combined electrical and seismic data sets, The Cryosphere, 5, 453–468, doi:10.5194/tc-5-453-2011, 2011.

Hausmann, H., Krainer, K., Brückl, E., and Mostler, W.: Internal structure and ice content of Reichenkar rock glacier (Stubai Alps, Austria) assessed by geophysical investigations, Permafrost Periglac., 18, 351–367, 2007.

Heap, M. J., Faulkner, D. R., Meredith, P. G., and Vinciguerra, S.: Elastic moduli evolution and accompanying stress changes with increasing crack damage: implications for stress changes around fault zones and volcanoes during deformation, Geophys. J. Int., 183, 225–236, doi:10.1111/j.1365-246X.2010.04726.x, 2010.

Hilbich, C.: Time-lapse refraction seismic tomography for the detection of ground ice degradation, The Cryosphere, 4, 243–259, doi:10.5194/tc-4-243-2010, 2010.

Ikeda, A.: Combination of Conventional Geophysical Methods for Sounding the Composition of Rock Glaciers in the Swiss Alps, Permafrost Periglac., 17, 35–48, 2006.

IPCC: IPCC Fourth Assessment Report. Climate Change 2007 – The Physical Science Basis, Cambridge University Press, Cambridge, 2007.

Jaeger, C.: Rock mechanics and engineering, Cambridge University Press, Cambridge, 536 pp., 2009.

Johnston, J. E. and Christensen, N. I.: Seismic Anisotropy of Shales, J. Geophys. Res.-Sol. Ea., 100, 5991–6003, 1995.

Kenner, R., Phillips, M., Danioth, C., Denier, C., Thee, P., and Zgraggen, A.: Investigation of rock and ice loss in a recently deglaciated mountain rock wall using terrestrial laser scanning: Gemsstock, Swiss Alps, Cold Reg. Sci. Technol., 67, 157–164, doi:10.1016/j.coldregions.2011.04.006, 2011.

King, M. S.: Wave Velocities in Rocks as a Function of Changes in Overburden Pressure and Pore Fluid Saturants, Geophysics, 31, 50–73, 1966.

King, M. S.: Acoustic velocities and electrical properties of frozen sandstones and shales, Can. J. Earth Sci., 14, 1004–1013, 1977.

King, M. S.: The influence of clay-sized particles on seismic velocity for Canadian Arctic permafrost, Can. J. Earth Sci., 21, 19–24, 1984.

King, M. S., Zimmermann, R. W., and Corwin, R. F.: Seismic and electrical properties of unconsolidated permafrost, Geophys. Prospec., 36, 349–364, doi:10.1111/j.1365-2478.1988.tb02168.x, 1988.

Kneisel, C., Hauck, C., Fortier, R., and Moorman, B.: Advances in geophysical methods for permafrost investigations, Permafrost Periglac., 19, 157–178, doi:10.1002/ppp.616, 2008.

Krautblatter, M.: Rock permafrost geophysics and its explanatory power for permafrost-induced rockfalls and rock creep: a perspective, 9th International Conference on Permafrost, Fairbanks, Alaska, US, 999–1004, 2008.

Krautblatter, M.: Detection and quantification of permafrost change in alpine rock walls and implications for rock instability, Math.-Nat. Fakultät, Univerität Bonn, Bonn, 164 pp., 2009.

Krautblatter, M.: Patterns of multiannual aggradation of permafrost in rock walls with and without hydraulic interconnectivity (Steintälli, Valley of Zermatt, Swiss Alps), in: Landform – Structure, Evolution, Process Control, edited by: Otto, J. C. and Dikau, R., Lect. Notes Earth Sci., Springer, Heidelberg, 115, 199–219, 2010.

Krautblatter, M. and Hauck, C.: Electrical resistivity tomography monitoring of permafrost in solid rock walls, J. Geophys. Res.-Earth, 112, F02S20, doi:10.1029/2006jf000546, 2007.

Krautblatter, M., Heißel, G., Moser, M., Nittel, P., and Verleysdonk, S.: Bliggferner – Tomographie einer Massenbewegung im Permafrostbereich zur Einschätzung des Gefährdungspotentials, 11. Geoforum Umhausen, Tirol, 10–12, 2009.

Krautblatter, M., Verleysdonk, S., Flores-Orozco, A., and Kemna, A.: Temperature-calibrated imaging of seasonal changes in permafrost rock walls by quantitative electrical resistivity tomography (Zugspitze, German/Austrian Alps), J. Geophys. Res.-Earth, 115, F02003, doi:10.1029/2008JF001209, 2010.

Krautblatter, M., Huggel, C., Deline, P., and Hasler, A.: Research perspectives for unstable high-alpine bedrock permafrost: measurement, modelling and process understanding, Permafrost Periglac., 23, 80–88, 2012.

Krus, M.: Feuchtetransport und Speicherkoeffizienten poröser mineralischer Baustoffe – theoretische Grundlagen und neue Meßtechniken, Fakultät für Bauingenieur- und Vermessungswesen, University of Stuttgart, Stuttgart, 1995.

Kurfurst, P. J. and Hunter, J. A.: Field and laboratory measurements of seismic properties of permafrost, P. Sym. Permafrost Geophys., 1977, 1–15, 1977.

Leclaire, P., Cohen-Ténoudji, F., and Aguirre-Puente, J.,: Extension of Biot's theory of wave propagation to frozen porous media, J. Acoust. Soc. Am., 96, 3753–3768, 1994.

Lo, T. W., Coyner, K. B., and Toksoz, M. N.: Experimental-Determination of Elastic-Anisotropy of Berea Sandstone,

Chicopee Shale, and Chelmsford Granite, Geophysics, 51, 164–171, 1986.
Lock, G. S. H.: The growth and decay of ice, Studies in Polar Research, University Press, Cambridge, 2005.
Matsuoka, N.: Mechanisms of Rock Breakdown by Frost Action – an Experimental Approach, Cold Reg. Sci. Technol., 17, 253–270, 1990.
Matsuoka, N. and Murton, J.: Frost weathering: Recent advances and future directions, Permafrost Periglac., 19, 195–210, 2008.
Matsuoka, N., Hirakawa, K., Watanabe, T., Haeberli, W., and Keller, F.: The role of diurnal, annual and millenial freeze-thaw cycles in controlling alpine slope stability, 7th International Conference on Permafrost, Yellowknife, Canada, 711–717, 1998.
Maurer, H. and Hauck, C.: Instruments and methods – Geophysical imaging of alpine rock glaciers, J. Glaciol., 53, 110–120, 2007.
Mavko, G., Mukerji, T., and Dvorkin, J.: The Rock Physics Handbook, 2nd Edn., Cambridge University Press, Cambridge, 525 pp., 2009.
McGinnis, L. D., Nakao, K., and Clark, C. C.: Geophysical identification of frozen and unfrozen ground, Antarctica, 2nd International Conference on Permafrost, Northamerican Contribution, Yakutsk, USSR, 136–146, 1973.
Murton, J. B., Coutard, J. P., Lautridou, J. P., Ozouf, J. C., Robinson, D. A., Williams, R. B. G., Guillemet, G., and Simmons, P.: Experimental design for a pilot study on bedrock weathering near the permafrost table, Earth Surf. Process. Landf., 25, 1281–1294, 2000.
Murton, J. B., Coutard, J. P., Lautridou, J. P., Ozouf, J. C., Robinson, D. A., and Williams, R. B. G.: Physical modelling of bedrock brecciation by ice segregation in permafrost, Permafrost Periglac., 12, 255–266, doi:10.1002/ppp.390, 2001.
Murton, J. B., Peterson, R., and Ozouf, J. C.: Bedrock fracture by ice segregation in cold regions, Science, 314, 1127–1129, 2006.
Musil, M., Maurer, H., Green, A. G., Horstmeyer, H., Nitsche, F., Vonder Mühll, D., and Springman, S.: Shallow seismic surveying of an Alpine rock glacier, Geophysics, 67, 1701–1710, 2002.
Nakano, Y., Smith, M., and Martin, R. J.: Ultrasonic Velocities of Dilatational and Shear Waves in Frozen Soils, Water Resour. Res., 8, 1024–1030, 1972.
Nogués-Bravo, D., Araújo, M. B., Errea, M. P., and Martínez-Rica, J. P.: Exposure of global mountain systems to climate warming during the 21st Century, Global Environ. Chan., 17, 420–428, 2007.
NRC-Permafrost-Subcommitee: Glossary of Permafrost and related ground-ice terms, NRC Technical Memorandum, 142, 1–156, 1988.
Nur, A. and Simmons, G.: Effect of Saturation on Velocity in Low Porosity Rocks, Earth Planet. Sci. Lett., 7, 183–193, 1969.
Pandit, B. I. and King, M. S.: A study of the effects of pore-water salinity on some physical properties of sedimentary rocks at permafrost temperatures, Can. J. Earth Sci., 16, 1566–1580, 1979.
Pearson, C., Murphy, J., and Hermes, R.: Acoustic and Resistivity Measurements on Rock Samples Containing Tetrahydrofuran Hydrates - Laboratory Analogs to Natural-Gas Hydrate Deposits, J. Geophys. Res.-Sol. Ea., 91, 14132–14138, 1986.
Ravanel, L. and Deline, P.: Climate influence on rockfalls in high-Alpine steep rockwalls: The north side of the Aiguilles de Chamonix (Mont Blanc massif) since the end of the "Little Ice Age", Holocene, 21, 357–365, doi:10.1177/0959683610374887, 2010.
Remy, J. M., Bellanger, M., and Homandetienne, F.: Laboratory Velocities and Attenuation of P-Waves in Limestones During Freeze-Thaw Cycles, Geophysics, 59, 245–251, 1994.
Roethlisberger, H.: Seismic refraction soundings in permafrost near Thule, greenland, Proceedings of the first International Symposium on Arctic Geology, Calgary, Alberta, 1960, 970–980, 1961.
Sass, O.: Rock moisture measurements: Techniques, results, and implications for weathering, Earth Surf. Proc. Land., 30, 359–374, 2005.
Scott, W. J., Sellmann, P. V., and Hunter, J. A.: Geophysics in the study of permafrost, in: Geotechnical and Environmental Geophysics, edited by: Ward, S., Society of Exploration Geophysicists, Tulsa, 355–384, 1990.
Siewert, M., Krautblatter, M., Christiansen, H. H., and Eckersdorfer, M.: Arctic rockwall retreat rates estimated using laboratory-calibrated ERT measurements of talus cones in Longyeardalen, Svalbard Earth Surf. Proc. Land., in press, doi:10.1002/esp.3297, 2012.
Sondergeld, C. H. and Rai, C. S.: Velocity and resistivity changes during freeze-thaw cycles in Berea sandstone, Geophysics, 72, E99–E105, 2007.
Takeuchi, S. and Simmons, G.: Elasticity of Water-Saturated Rocks as a Function of Temperature and Pressure, J. Geophy. Res.-Sol. Ea., 78, 3310–3320, 1973.
Tharp, T. M.: Conditions for crack propagation by frost wedging, Geol. Soc. Am. Bull., 99, 94–102, 1987.
Thomsen, L.: Weak Elastic-Anisotropy, Geophysics, 51, 1954–1966, 1986.
Tiab, D. and Donaldson, E. C.: Petrophysics. Theory and practice of measuring reservoir rock and fluid transport properties, 2nd Edn., Elsevier, Oxford, 926 pp., 2004.
Tice, A. R., Burrous, A. M., and Anderson, D. M.: Determination of unfrozen water in frozen soil by pulsed nuclear magnetic resonance, 3rd International Conference on Permafrost, Edmonton, Canada, 1978, 149–155, 1978.
Timur, A.: Velocity of compressional waves in porous media at permafrost temperatures, Geophysics, 33, 584–595, doi:10.1190/1.1439954, 1968.
Toksöz, M. N., Cheng, C. H., and Timur, A.: Velocities of Seismic-Waves in Porous Rocks, Geophysics, 41, 621–645, 1976.
Verleysdonk, S., Krautblatter, M., and Dikau, R.: Sensitivity and path dependence of mountain permafrost systems, Geogr. Ann., 93A, 113–135, doi:10.1111/j.1468-0459.2011.00423.x, 2011.
Vernik, L. and Nur, A.: Ultrasonic Velocity and Anisotropy of Hydrocarbon Source Rocks, Geophysics, 57, 727–735, 1992.
Vlahou, I. and Worster, M. G.: Ice growth in a spherical cavity of a porous medium, J. Glaciol., 56, 271–277, 2010.
Walder, J. and Hallet, B.: A Theoretical-Model of the Fracture of Rock During Freezing, Geol. Soc. Am. Bull., 96, 336–346, 1985.
Walder, J. S. and Hallet, B.: The Physical Basis of Frost Weathering – toward a More Fundamental and Unified Perspective, Arctic Alpine Res., 18, 27–32, 1986.
Wang, Z. J.: Fundamentals of seismic rock physics, Geophysics, 66, 398–412, 2001.
Wassermann, J., Senfaute, G., Amitrano, D., and Homand, F.: Evidence of dilatant and non-dilatant damage processes in oolitic iron ore: P-wave velocity and acoustic emission analyses, Geophys. J. Int., 177, 1343–1356, doi:10.1111/j.1365-246X.2008.04017.x, 2009.

Winkler, K. W.: Frequency-dependent ultrasonic properties of high-porosity sandstones, J. Geophy. Res., 88, 9493–9499, doi:10.1029/JB088iB11p09493, 1983.

Wohlenberg, J.: 1.2 Densities of rocks, in: Springer Materials – The Landolt-Börnstein Database, available at: http://www.springermaterials.com, edited by: Angenheister, G., 2012.

Wyllie, M. R. J., Gregory, A. R., and Gardner, L. W.: Elastic wave velocities in heterogeneous and porous media, Geophysics, 21, 41–70, 1956.

Wyllie, M. R. J., Gregory, A. R., and Gardner, L. W.: An experimental investigation of factors effecting elastic wave velocities in porous media, Geophysics, 23, 459–493, 1958.

Zimmerman, R. W. and King, M. S.: The effect of the extent of freezing on seismic velocities in unconsolidated permafrost, Geophysics, 51, 1285–1290, 1986.